Journal Pre-proof

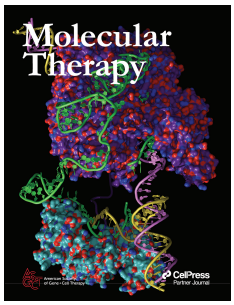

Balancing activation and costimulation of CAR tunes signaling dynamics and enhances therapeutic potency

Yanting Duan, Jiangqing Chen, Xianhui Meng, Longwei Liu, Kai Shang, Xiaoyan Wu, Yajie Wang, Zihan Huang, Houyu Liu, Yanjie Huang, Chun Zhou, Xiaofei Gao, Yingxiao Wang, Jie Sun

PII: S1525-0016(22)00506-8

DOI: https://doi.org/10.1016/j.ymthe.2022.08.018

Reference: YMTHE 5902

To appear in: *Molecular Therapy*

Received Date: 11 March 2022

Accepted Date: 25 August 2022

Please cite this article as: Duan Y, Chen J, Meng X, Liu L, Shang K, Wu X, Wang Y, Huang Z, Liu H, Huang Y, Zhou C, Gao X, Wang Y, Sun J, Balancing activation and costimulation of CAR tunes signaling dynamics and enhances therapeutic potency, *Molecular Therapy* (2022), doi: https://doi.org/10.1016/j.ymthe.2022.08.018.

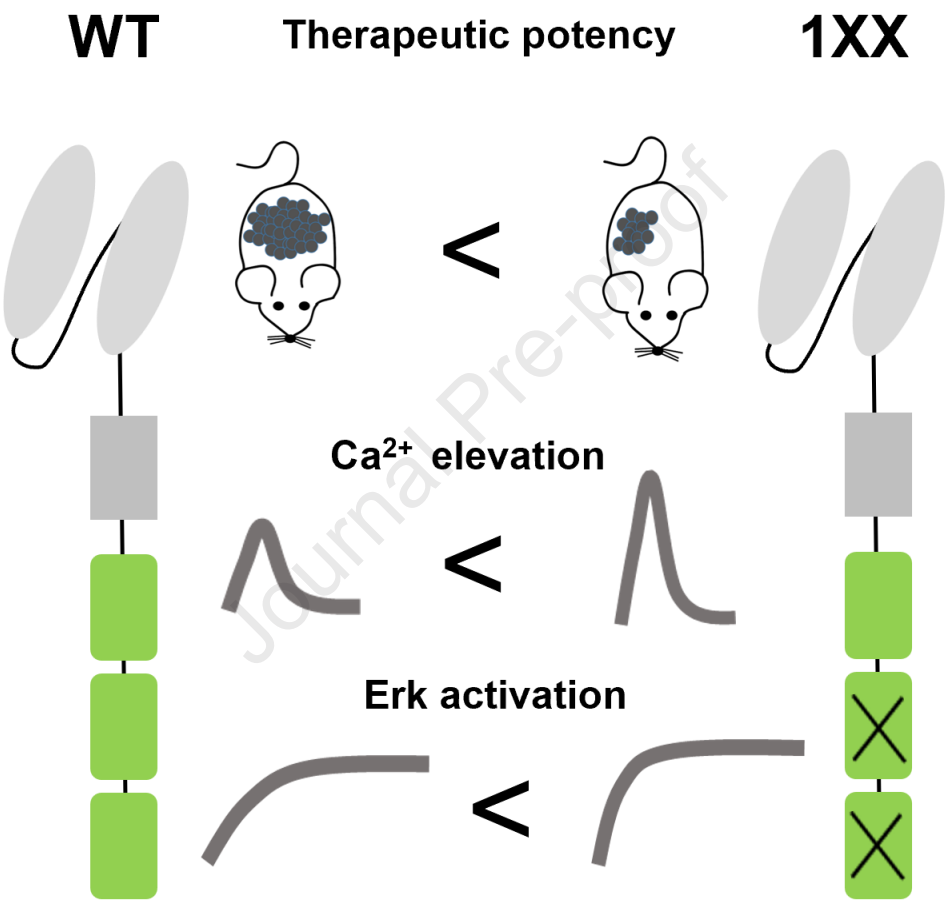

Balancing activation and costimulation of CAR tunes signaling dynamics and enhances therapeutic potency

Yanting Duan[1,2,3#], Jiangqing Chen[1,2,3#], Xianhui Meng[1,2,3], Longwei Liu[4], Kai Shang[1,2,3], Xiaoyan Wu[1,2,3], Yajie Wang[1,2,3], Zihan Huang[1,2,3], Houyu Liu[1,2,3], Yanjie Huang[5], Chun Zhou[6], Xiaofei Gao[5], Yingxiao Wang[4], Jie Sun[1,2,3]

Author details

1, Bone Marrow Transplantation Center of the First Affiliated Hospital and Department of Cell Biology, Zhejiang University School of Medicine, 866 Yuhangtang Road, Hangzhou 310058, China

2, Liangzhu Laboratory, Zhejiang University Medical Center, 1369 West Wenyi Road, Hangzhou 311121, China

3, Institute of Hematology, Zhejiang University & Zhejiang Engineering Laboratory for Stem Cell and Immunotherapy, Hangzhou 310058, Zhejiang, China

4, Department of Bioengineering, Institute of Engineering in Medicine, University of California, San Diego, CA 92093, USA

5, Key Laboratory of Structural Biology of Zhejiang Province, School of Life Sciences, Westlake University, Hangzhou 310058, China

6, School of Public Health and Sir Run Run Shaw Hospital, Zhejiang University School of Medicine, Hangzhou 310058, China

# These authors contributed equally: Yanting Duan, Jiangqing Chen

Jie Sun: sunj4@zju.edu.cn (Corresponding author).

Keywords: CAR, CD3ζ, ITAM, CD28, 1XX, CD19, AXL, immunotherapy

Abstract

CD19-targeting chimeric antigen receptors (CARs) with CD28 and CD3ζ signaling domains have been approved by the US FDA for treating B cell malignancies. Mutation of immunoreceptor tyrosine-based activation motifs (ITAMs) in CD3ζ generated a single-ITAM containing 1XX CAR, which displayed superior anti-tumor activity in a leukemia mouse model. Here we investigated whether the 1XX design could enhance therapeutic potency against solid tumors. We constructed both CD19- and AXL-specific 1XX CARs and compared their *in vitro* and *in vivo* functions with their wild type (WT) counterparts. 1XX CARs showed better anti-tumor efficacy in both pancreatic and melanoma mouse models. Detailed analysis revealed that 1XX CAR-T cells persisted longer *in vivo* and had a higher percentage of central memory cells. With fluorescence resonance energy transfer (FRET)-based biosensors, we found that decreased ITAM numbers in 1XX resulted in similar 70-kDa zeta-chain associated protein (ZAP70) activation, while 1XX induced higher Ca^{2+} elevation and faster extracellular signal-regulated kinase (Erk) activation than WT CAR. Thus, our results confirmed the superiority of 1XX against two targets in different solid tumor models and shed light on the underlying molecular mechanism of CAR signaling, paving the way for the clinical applications of 1XX CARs against solid tumors.

Introduction

The adoptive transfer of chimeric antigen receptor (CAR)-T cells has achieved great success in treating hematological malignancies and the US FDA has approved four CD19-specific CAR-T products and two products targeting BCMA.[1,2] On the other hand, it is generally recognized that the application of CAR-T in solid tumors has been impeded by many factors, including a lack of tumor-exclusive antigen, inefficient tumor trafficking and immunosuppressive tumor microenvironment.[3] Various strategies have been developed in combination of CAR to overcome these hurdles, such as co-expression of cytokines,[4,5] secretion of scFv against PD-1,[6] secretion of BiTEs to recruit bystander T cells[7] and the use of IL-7/CCL-19 to increase trafficking.[8] However, the CAR design itself may still not be optimized to fully harness the power of T cells.

In addition to the activation signals from a T cell receptor (TCR), T cells integrate signals from costimulatory/coinhibitory receptors and cytokine receptors through a complex signaling network to direct multiple functions, such as proliferation, cytotoxicity, cytokine secretion and differentiation.[9] These functions need to be balanced to achieve optimal long-term anti-tumor effects. After antigen binding, CD28-based second-generation CARs transduce signals through the costimulatory domain from CD28 and the activation domain from CD3ζ, which comprises three immunoreceptor tyrosine-based activation motifs (ITAMs). Both pathways highly depend on the activity of Lck kinase. Each ITAM in CD3ζ after being phosphorylated by Lck recruits ZAP70 kinase so that ZAP70 can be phosphorylated by Lck.[10] ZAP70 activation further phosphorylates adaptor LAT at the membrane, which forms a signaling network with various proteins, such as Grb2/Sos and PLCγ. PLCγ catalyzes the formation of two important second messengers, DAG and IP3.[11] IP3 binds to receptors at the ER to release large amount of Ca^{2+}, while both DAG and Grb2/Sos could activate Erk through Ras.[12,13] Meanwhile, after being phosphorylated by Lck, the

CD28 cytosolic domain can recruit and activate PI3K.[14] PIP3 produced by PI3K binds to the PH domain of Itk, recruiting Itk to the membrane. Itk can directly interact with PLCγ and activate it.[15] Thus, both pathways can modulate downstream Ca^{2+} and Erk activities.

A single ITAM-containing 1XX CAR design with calibrated activation potential has been shown to have superior anti-tumor activity in a leukemia mouse model by balancing activation and costimulatory signals.[16] Here we investigated whether this design benefits CAR-T therapy against solid tumors. We also quantified the molecular activities in CAR-T cells with high temporal resolution by fluorescence resonance energy transfer (FRET) biosensors. Based on the importance of the signaling molecules and the availability of biosensors, we chose ZAP70, Ca^{2+} and Erk biosensors[17-19] to reveal differences in signaling dynamics induced by 1XX compared to WT CAR.

Results

CD19-1XX CAR-T cells had lower cytotoxicity against Panc-1 cells *in vitro*

In the NALM6 leukemia mouse model, CD19-1XX CAR-T cells had shown superior anti-tumor activity than the CD19-WT cells.[16] In this study, we first investigated whether the CD19-1XX CAR-T cells controlled solid tumors better than the CD19-WT cells. With CRISPR/Cas9-mediated gene targeting,[20] we integrated CD19-WT or CD19-1XX CAR at the specific *TRAC* locus to generate CAR-T cells (Figure 1a, Figure S1a). The resulting CAR-T cells have similar knock-in efficiency (Figure 1b) and surface expression of CARs (Figure 1c). To have a direct comparison of the two CD19-specific CAR-T cells, we ectopically expressed the human CD19 antigen in the pancreatic cell line Panc-1 for both the *in vitro* killing assay and the *in vivo* xenograft model (Figure S1b). With Panc-1^{CD19+} cells as targets, CD19-1XX CAR-T cells displayed significantly lower cytotoxicity than CD19-WT cells at different E:T ratios in an 18h killing assay (Figure 1d, e), which was confirmed by results from two additional donors (Figure S1c, d). Data

summarized from three donors showed that 24h after antigen stimulation, CD19-1XX and CD19-WT CAR-T cells secreted similar amount of IL-2, IFNγ and TNFα (Figure 1f, Figure S1e). In addition, our CFSE-based assay showed that 72h after antigen stimulation, the proliferation capacity of CD19-1XX was not statistically different from that of CD19-WT, though it had a higher trend (Figure 1g, h, Figure S1f). In summary, CD19-1XX cells displayed lower cytotoxicity, similar cytokine secretion and antigen-dependent proliferation *in vitro*.

CD19-1XX CAR-T cells showed better anti-tumor activity in a pancreatic tumor model

We next compared the anti-tumor activity of two CD19 CAR-T cells in a xenograft pancreatic cancer model, where Panc-1^{CD19+} cells were subcutaneously injected in the right flank of NSG mice (Figure 2a). We used a low dose of CAR-T cells (1×10^6) with similar transduction efficiency (Figure 1b) to better compare T cell potency in the CAR stress test.[21] Though both CAR-T cells inhibited initial tumor growth, mice injected with CD19-WT CAR-T cells started to relapse around day 29 while mice treated with CD19-1XX CAR-T cells relapsed around day 46 (Figure 2b). At day 53, the average tumor volume of mice with CD19-1XX CAR-T cells was significantly smaller than that of mice injected with CD19-WT cells (Figure 2b, c). As CAR targeting *TRAC* locus knocked out the CD3 expression, we used antibodies against human CD4 or CD8 molecule to stain for human CAR-T cells in the tumor tissue. Our results revealed the existence of $CD4^+$ and $CD8^+$ T cells in the tissue even at day 53, albeit at a very low percentage (Figure 2d-f). Even though the percentage of either $CD4^+$ or $CD8^+$ T cells was not statistically different between CD19-1XX and CD19-WT groups, CD19-1XX groups had a trend of more $CD4^+$ and $CD8^+$ T cells (Figure 2e, f). In an independent *in vivo* experiment using CAR-T cells from a different donor (Figure S2a-c), we didn't observe differences in tumor growth, possibly because that donor was particularly potent, masking subtle differences. However, CD19-1XX group had more splenic total

CAR-T cells as well as more $CD4^+$ CAR-T cells than the CD19-WT group in mice 53 days after CAR-T infusion (Figure S2d; Figure 2g, h). Though no statistical difference, the CD19-1XX group displayed a lower percentage of PD-1^+LAG-3^+ exhausted cells in both $CD4^+$ and $CD8^+$ populations (Figure S2e). Further phenotypic analysis of CAR-T cells demonstrated that the percentage and cell count of $CD8^+$ T_{EFF} ($CD45RA^+CD62L^-$) were higher in CD19-1XX than CD19-WT (Figure 2i, Figure S2f). For the $CD4^+$ population, CD19-1XX had a trend of more percentage of T_{CM} ($CD45RA^-CD62L^+$), but less percentage of T_{EFF} (Figure 2j, Figure S2g).

1XX modification of AXL CAR enhanced its anti-tumor activity in a melanoma model

After we confirmed that CD19-1XX cells were better than CD19-WT in both leukemia [16] and solid tumor models, we further investigated whether the 1XX design is also beneficial for CARs targeting antigens expressed naturally in solid tumors. AXL is a tyrosine kinase receptor, commonly overexpressed in both hematological malignancies and solid tumors.[22] Human melanoma cell line A375 was shown to have a high expression of AXL antigen (Figure S3a). We constructed a CAR targeting AXL (AXL-WT) using the scFv from an DAXL-88 antibody we reported before (Figure S3b), and also generated a 1XX-modified AXL-specific CAR for comparison (Figure 3a). Expression of AXL-WT and AXL-1XX CAR was also similar (Figure 3b, c). AXL-1XX induced lower killing of A375 cells than AXL-WT CAR-T cells (Figure 3d, e; Figure S3c, d). Meanwhile, data summarized from three donors suggested that AXL-1XX and AXL-WT CAR-T cells had similar cytokine secretion (Figure 3f, Figure S3e). The CFSE-based assay showed that AXL-1XX has stronger proliferative capability than AXL-WT upon antigen-stimulation (Figure 3g, h; Figure S3f).

Then we compared their anti-tumor activity in a xenograft melanoma model, where A375 cells were subcutaneously injected in the right flank of NSG mice (Figure 4a). Interestingly, AXL-

WT CAR-T failed to control tumor growth when injected at a low 1×10^6 dose while AXL-1XX CAR-T cells significantly reduced tumor size at the same dose (Figure 4b-e). We confirmed this finding in an independent experiment with CAR-T cells produced from a different donor (Figure S4a-d). Our results revealed the existence of $CD4^+$ and $CD8^+$ T cells in the tissue at day 14 (Figure 4e). The percentage of $CD4^+$ T cells was not statistically different between the AXL-1XX and AXL-WT groups, while the AXL-1XX groups had more percentage of $CD8^+$ T cells (Figure 4f, g). The analysis of CAR-T cells extracted from mice revealed that the total number of the AXL-1XX CAR-T cells was about 110 fold more than that of the AXL-WT cells (Figure S4e). The dramatic increase of cell numbers from AXL-1XX CAR-T cells were seen in both $CD4^+$ (116 fold) and $CD8^+$ populations (121 fold) (Figure 4h, i). Further phenotypic analysis showed that AXL-1XX CAR-T cells had a significantly higher percentage of central memory cells and lower percentage of effector cells in both $CD4^+$ and $CD8^+$ populations (Figure 4j, k). As the total CAR-T cells were much higher in 1XX, the total numbers of central memory cells and effector cells were both higher in mice injected with AXL-1XX cells (Figure S4g, h). Meanwhile, 1XX led to the trend of fewer percentage of PD-1^+LAG3^+ exhausted cells than AXL-WT cells (Figure S4f). To summarize, the comparison of AXL-1XX and AXL-WT was mostly consistent with the CD19-1XX and CD19-WT comparison. Although the 1XX design reduced CAR-T cytotoxicity *in vitro*, it enhanced the anti-tumor activity of CARs targeting two solid tumor models *in vivo*, which has more significance for CAR-T therapy.

1XX CAR induced higher Ca^{2+} level and faster Erk activation than WT CAR

Our previous work with the leukemia model indicated that CD19-1XX cells had a better anti-tumor activity because they were more persistent and comprised of increased numbers of memory cells.[16] It is intriguing how a simple 1XX calibration can have a profound impact on

cellular phenotypes and functions. To complement the global RNAseq comparison between CD19-1XX and CD19-WT,[16] we next compared CAR-mediated signaling dynamics in CD19-1XX and CD19-WT cells with different FRET biosensors. FRET biosensors enable monitoring of the molecular activity at a single cell level with high spatiotemporal resolution. Here, all the FRET changes of the biosensor in every cell was normalized to its unstimulated baseline level so we could directly compare antigen-induced activation.

As ZAP70 kinase directly binds phosphorylated ITAMs of TCR and CARs to get activated, the 1XX mutation might directly affect the activity of ZAP70. Using a recently developed ZAP70 FRET biosensor with improved dynamic range, ZAP70 activation dynamics can be observed in CAR-T cells upon antigen stimulation.[17] We expressed this biosensor together with either CD19-1XX or CD19-WT CAR, and performed live cell FRET imaging (Figure S5a). ZAP70 activation can be observed by the FRET biosensor after CAR-antigen interaction. The activation dynamics induced by CD19-1XX and CD19-WT CAR were not statistically different (Figure 5a-e, Figure S5b, c). However, CD19-1XX exhibited a trend of lower ZAP70 activity within the first 5min but eventually caught up with CD19-WT at 30mins. We next investigated cytosolic Ca^{2+} elevation[18] and Erk activation, as they are key signaling events downstream of both TCR/CD3ζ-ZAP70 and CD28-PI3K pathways and have profound effects on T cell functions through transcriptional regulation. Our results showed that Ca^{2+} elevation at 1.5min in 1XX cells was significantly higher than that in WT cells (Figure 5f-j, Figure S5d, e). Moreover, analysis of CAR-T cells transduced with Erk biosensors [19] revealed that CD19-1XX directed faster Erk activation than CD19-WT did upon target cell binding (Figure 5k-o, Figure S5f, g). We further analyzed the Shp1 recruitment and Lck activation in CAR-T cells. Our co-IP results showed that even though there was no significant difference of recruited Shp1 after antigen stimulation between WT and 1XX CAR, the

baseline CAR-associated Shp1 (Time 0) was lower in 1XX CAR group (Figure S6). With a FRET-based Lck biosensor to monitor Lck activity,[23] we showed that WT and 1XX induced little Lck activation upon antigen recognition and there was no statistical difference between these two groups (Figure S7). Thus, even though 1XX-induced a trend of reduced ZAP70 activity, it increased antigen-dependent Ca^{2+} elevation and sped up Erk activation, which were correlated with higher therapeutic potency.

Discussion

1XX design has been shown to be advantageous in the CD19 CAR context against leukemia. The most relevant translational question is whether 1XX modification is also beneficial against solid tumors. Though a prior study reported the 1XX design of a mesothelin-targeting CAR was effective in a pleural mesothelioma mouse model,[24] there was no direct comparison with its WT counterpart and the underlying molecular mechanisms were not investigated. Our study demonstrated that 1XX modification can enhance CAR-T cell efficacy against solid tumors in two different CAR settings and tumor models, suggesting this could be a general optimization strategy. The increased efficacy was attributed to the observations that CD19-1XX CAR-T cells extracted from leukemic mice were of higher number and had a higher percentage of $CD62^{+}CD45RA^{-}$ T_{CM} cells than CD19-WT cells.[16] In our study, we tried to isolate CAR-T cells from subcutaneous tumors to analyze their phenotype but we could not detect enough CAR-T cells (data not shown). This was most likely because we injected a low CAR-T cell dose and collected the tumor tissue at the very last time point. We chose a low CAR-T cell dose as a “stress test” for better comparison of T cells with different CAR constructs.[21] The low number of CAR-T cells in tumors was corroborated by in situ immunostaining of CAR-T cells. Quantitative analysis of immunostaining indicated a trend of more CD19-1XX cells than CD19-WT cells, which was consistent with the

results from the leukemic mouse model. Nevertheless, we could isolate enough CAR-T cells from the mouse spleen instead of tumors for detailed characterization. The 1XX mutation in AXL-CAR increased the number of total CAR-T cells by 110.5 fold, and these cells displayed an increased central memory phenotype and decreased exhaustion trend, which was consistent with the effect of 1XX modification on CD19 CAR.

1XX CAR-T cells have significantly lower cytotoxicity than WT CAR-T cells when killing Panc-1^{CD19+} cells. Previous data showed that CD19-1XX and CD19-WT CAR-T cells display similar cytotoxicity against leukemic NALM6 cells *in vitro*.[16] AXL-specific 1XX CAR-T cells also have decreased killing against A375 tumor cells. Thus it is possible that results of *in vitro* killing assays cannot predict *in vivo* anti-tumor activities of different CAR-T cells. Here, the 1XX design has already been combined with the TRAC-targeting of CAR to take advantage of two optimization methods.[20] Whether 1XX can be combined with other known therapeutic enhancement strategies, such as IL-12, PD-1 blocking scFv or IL-7/CCL19, to further enhance CAR-T performance against solid tumors, warrants further investigation.

RNAseq analysis of CD19-1XX and CD19-WT cells revealed their global transcriptional difference 24h after target recognition,[16] but how 1XX mutation leads to differential gene expression was still elusive. Here we employed different FRET biosensors to probe the signaling dynamics of three key molecules downstream CAR activation (Figure 6). Each ITAM from CD3ζ has two tyrosines, both of which need to be phosphorylated to recruit ZAP70 so that ZAP70 can be phosphorylated by Lck.[10] But singly-phosphorylated ITAMs was shown to instead recruit Shp1 phosphatase, which in turn inhibits Lck activity through negative feedback[25] (Figure 6). Indeed, before antigen stimulation CAR-associated Shp1 level was lower in 1XX CAR-T cells than that in WT cells (Figure S6a, b). Additional results assayed with FRET-based Lck biosensor showed

no statistical difference of induced Lck activation by 1XX and WT CARs (Figure S7a, b), which didn't exclude the possibility of enhanced Lck activity by 1XX CAR as the limited dynamic range of the Lck biosensor may mask the subtle difference in signaling dynamics.[23] Thus, 1XX with reduced ITAMs could possibly enhance Lck activity by decreasing the amount of singly-phosphorylated ITAMs and associated Shp1. The total ZAP70 activity of 1XX would be the net result of these two opposing effects, as reduced ITAM numbers decreased the amount of bound ZAP70, but increased the activation of bound ZAP70 by enhanced Lck activity. Our FRET data showed that even though ZAP70 activity in 1XX was not statistically different from that in WT, the trend was lower (Figure 5e).

If only the CD3ζ-ZAP70 pathway was considered, the 1XX mutation should not alter the Ca^{2+} and Erk activation through LAT. But in the context of CD28-based second generation CAR, CD28 cytosolic domain after being phosphorylated by Lck can also augment Ca^{2+} and Erk signaling through PI3K activation[12,13] (Figure 6). As 1XX can enhance Lck activity through reduced singly-phosphorylated ITAMs and associated Shp1,[26,27] CD28 phosphorylation by Lck in 1XX CAR may be strengthened, which promotes higher or faster PI3K activation[12,13] (Figure 6). Our FRET-based imaging revealed that 1XX resulted in significantly higher Ca^{2+} elevation and more rapid Erk activation than WT upon antigen binding (Figure 5), which was consistent with the prediction from a mathematical model.[25] Increased Ca^{2+} would bind to calcineurin and activate transcription factors of the NFAT family to regulate cytokine gene expression and other genes critical for the T cell functions.[28,29] Erk could further activate transcription factors, such as Elk-1 and AP-1.[30,31] Particularly, the Erk pathway was shown to be pivotal for both human memory Th17 cells and CD8 T cell differentiation,[32-34] suggesting that faster Erk activation kinetics of 1XX may be linked to CAR-T cell differentiation. Feucht et al.[16] compared the function of three CARs with

decreasing activation strength, WT, 1XX and XX3. 1XX resulted in the highest number of memory cells and XX3 CAR-T group had the least number of exhausted cells. Liu et al. showed that XX3 had much weaker ZAP70 activity than WT CAR upon antigen stimulation while they had similar Erk activity.[17] However, our data demonstrated that 1XX CAR had higher Erk activity than WT CAR while they had similar ZAP70 activity. Taken together, we speculate that the ZAP70 activation seems to be related to the exhaustion phenotype while the Erk activation seems to be related to the memory phenotype. Further investigation are needed to depict the relationship between signal strength and T-cell phenotypes.

Our study established the superior anti-tumor effect of 1XX CAR in two preclinical solid tumor models and revealed the delicate changes of signaling dynamics caused by 1XX CAR, paving the way for the clinical translation of 1XX CAR in treating solid tumors.

Materials and methods

Cells lines and culture conditions

Panc-1 cells were transduced to express human CD19 as described previously,[21,35] Panc-1^{CD19+} cells were sorted by Flow Cytometry. Panc-1^{CD19+}, A375 cells were transduced to express firefly luciferase, and (FFLuc)-2A-green fluorescent protein (GFP), and GFP^{+} cells were sorted by Flow Cytometry. Panc-1, A375, 293T and NIH/3T3 were cultured in Dulbecco's modified Eagle medium (DMEM, Gibco), with 10% FBS (Vistech) and 1% penicillin/streptomycin (Gibco). Jurkat cells were cultured in a RPMI-1640 medium (Gibco) with 10% FBS and 1% penicillin/streptomycin.

RNP production

RNPs were produced by complexing gRNA and Cas9 protein. Modified guide RNAs (gRNAs) was synthesized by GeneScript. Guide RNAs were reconstituted at 1μg/μL in RNase free water,

Cas9 proteins were produced by our lab as described in our previous work,[36] In brief, they were complexed in 2:1 gRNA to Cas9 molar ratio at room temperature for 20 min then electroporated into T cells immediately after complexing.[36]

Plasmid construction

Based on pAAV-TRAC-1928z plasmid (as described in our previous work,[36] named as CD19-WT), we designed and cloned the pAAV-TRAC-1928z-1XX (named as CD19-1XX). Briefly, the CD19 CAR comprises a single chain variable fragment[20] scFv specific for the human CD19 (AXL CAR comprises a single chain variable fragment of anti-AXL[37] specific binding to human AXL), preceded by a CD8a leader peptide and followed by CD28 hinge, transmembrane and intracellular regions and CD3ζ intracellular domain. The CAR cDNA is followed by the bovine growth hormone polyA signal (bGHpA). In brief, pAAV-TRAC-AXL28z/1XX plasmids were constructed with the following primers. AAV-AXL-forward primer: GTGGAGGAGAATCCCGGCCCCatggctctcccagtgactgccctactg; AAV-AXL-reverse primer: GCAACTAGAAGGCACAGTCGcctagggatttagcgagggggcagggcctg, the anti-AXL scFv fragment was obtained by PCR and inserted into pAAV-TRAC-1928z-WT or pAAV-TRAC-1928z-1XX plasmid which was digested out as 1928z-WT or 1928z-1XX fragments by NcoI/AvrII, respectively. The pAAV-TRAC-AXL28z/1XX plasmids were prepared using standard molecular biology techniques as described previously.[16] The Lenti-ZAP70-BS-CD19 CAR, Lenti-Ca^{2+}-BS-CD19 CAR and Lenti-Erk-BS-CD19 CAR plasmids were constructed as in our previous work[17] for FRET analysis. Lenti-Lck-BS-CD19 CAR plasmids were constructed as in previous work.[23]

Isolation and expansion of human T cells

Human PBMCs were isolated from the peripheral blood of healthy volunteers. Ethical permission was granted by the School of Medicine, Zhejiang University. All blood samples were handled

following the required ethical and safety procedures. Peripheral blood mononuclear cells were isolated by ficoll density gradient centrifugation (Dakewe) and T cells were purified using the Pan T Cell Isolation Kit (Miltenyi Biotec), and stimulated with CD3/CD28 T cell Activator Dynabeads (Thermofisher) as described previously,[20] then cultured in X-VIVO 15 Serum-free Hematopoietic Cell Medium (Lonza), which was supplemented with 10% fetal bovine serum (Vistech), 5ng/mL IL7 (interleukin-7) and 5ng/ml IL15 (interleukin-15) (Novoprotein) for the experiments. The medium was changed every 2 days, and cells were plated at 10^6 cells/mL. After stimulated for 48 h, human T cells were debeaded for gene targeting experiments.

CAR-T cell production

RNPs were electroporated into T cells 2 days after CD3/CD28 bead stimulation. Before electroporation, debeaded T cells were resuspended in X-VIVO 15 medium. For each reaction, 3×10^6 cells were mixed with 3.6 μL (80 pmol) RNPs in a total volume of 120 μL and transferred to a 120ul cuvette and electroporated with an Cell Electroporator (CELETRIX). Thirty minutes later, the AAV virus (MOI=1×10^5) (Vigene Biosciences, China) was added. Following electroporation, cells were immediately transferred into the culture medium (X-VIVO 15 with 10% FBS and 1% penicillin/streptomycin). Two hours later, IL-7 (5 ng/mL) and IL-15 (5 ng/mL) were added. Then the medium was changed every 48 h. Seven days after electroporation, cells were harvested for fluorescence-activated cell sorting (FACS) analysis to determine the knock-in efficiency in each condition.

Flow cytometry

The following fluorophore-conjugated antibodies were used. For CD19 CAR staining, an Alexa Fluor 647 AffiniPure F(ab')2 Fragment Goat Anti-Mouse IgG was used (Jackson ImmunoResearch); for AXL CAR staining, an Alexa Fluor 647 AffiniPure anti-HA tag Goat Anti-

Mouse IgG was used (BD Bioscience). A375 stained with anti-AXL PE-conjugated antibodies (FAB154P, R&D); and the DAXL-88 (anti-AXL) binding assay used Alexa Fluor 647 AffiniPure anti-Fc tag Goat Anti-Human IgG (410711, BioLegend). Anti-Human CD4 antibody (BD, Horizon, BUV395), anti-Human CD8 antibody (BD, Pharmin, APC-CY^{TM}7), anti-Human CD279(PD-1) antibody (Invitrogen, eBioscience, PE-Cyanine7), anti-Human CD223(LAG-3) antibody (Invitrogen, eBioscience, Percp-efluor^{TM}710), anti-Human CD45RA antibody (Invitrogen, eBioscience, FITC), anti-Human CD62L antibody (Invitrogen, eBioscience, efluor450). For cell counting, CountBright Absolute Counting Beads were added (Invitrogen) according to the manufacturer's instructions. For *in vivo* experiments, Fc receptors were blocked using FcR Blocking Reagent, mouse (Miltenyi Biotec). CytoFLEX (Beckman) was used with FlowJo 7.6 software for analysis. All FACS plots presenting CAR-T cell phenotype data were conducted on gated APC positive CAR-T cells. For Co-immunoprecipitation assay, anti-HA magnetic beads (MCE, HY-K020) were used according to the manufacturer's instructions. For western blot assay, anti-HA (Cell Signaling Technology, 3724S), anti-Shp1 (Cell Signaling Technology, 3759S) and anti-GAPDH (Cell Signaling Technology, 5174S) were 1:1000 dilution, horseradish peroxidase conjugated secondary Abs (Goat-anti-Rabbit from Thermo Scientific) was 1:5000 dilution.

Antigen stimulation and cytokines analysis assay

Nine days after gene targeting, the CAR-T cells and irradiated target cells NIH/3T3^{CD19+} or A375 were cocultured at an E:T ratio of 4:1 without the addition of exogenous cytokines for 24 h, then cell culture supernatants were harvested and analyzed using a BD Cytometric Bead Array (CBA) Human Soluble Protein Master Buffer Kit (BD Biosciences) according to the manufacturer's instructions. The detection reagent is a mixture of phycoerythrin (PE)-conjugated antibodies, which provides a fluorescent signal in proportion to the amount of bound analyte. Soluble cytokine

can be measured using flow cytometry to identify particles with fluorescence characteristics of both the bead and the detector.

Proliferation assay

For the proliferation assay, CAR-T cells were labeled with Carboxyfluorescein diacetate succinimidyl ester (CFSE) using a kit from Beyotime. Briefly, cells were resuspended in RPMI 1640 with 10% FBS at a final concentration of 5×10^6 cells/mL, and CFSE solution was added at the suggested working concentration. The CAR-T cells were incubated at 37 °C for 10 min, and then washed three times with RPMI 1640 with 10% FBS. CFSE-labeled cells were further plated in 24-well plates, co-cultured with irradiated $3T3^{CD19+}$ or A375 cells (E:T=4:1) for 72 h. Unstimulated but CFSE-labeled CAR-T cells served as the control. 72h later CAR-T cells stained with CFSE were analyzed by CytoFLEX (Beckman) with FlowJo 7.6 software.

Cytotoxicity assay

Nine days after gene targeting, CAR-T cells were collected for luciferase-based cytotoxicity assay using FFluc-GFP $Panc\text{-}1^{CD19+}$ or A375 as target cells. The target (T) and effector (E) cells were co-cultured in triplicates at indicated E/T ratios using black 96-well flat plates with 2.5×10^4 target cells in a total volume of 100 μL per well in X-vivo 15 medium. Target cells alone were plated at the same cell density to determine the maximal luciferase expression (relative light units (RLU)); 18 h later, 100 μL luciferase substrate (Goldbio) was directly added to each well. Emitted light was detected in a luminescence plate reader. Lysis percentage was determined as $(1-(RLUsample)/(RLUmax)) \times 100$.

Immunofluorescence of tumor tissues

The mice were euthanized by carbon dioxide (CO_2) inhalation, and the tumors were harvested and fixed in 4% paraformaldehyde. Tumor tissue were sectioned for anti-CD4 (GB13064-1, Servicebio)

and anti-CD8 (GB13068, Servicebio) staining. All procedures followed the manufacturer's protocol. In brief, tumor tissue slides were incubated at 65℃ for 1h, blocked with PBS containing 3% BSA for 30 min at room temperature, and then incubated with the primary antibody at 4℃ overnight. The secondary antibody was incubated at room temperature for 50 min in dark conditions. Then slides were incubated with DAPI solution at room temperature for 10 min in dark conditions. Images were acquired by fluorescent microscopy. The nucleus is blue by labeling with DAPI. Positive cells are green or red according to the fluorescent labels used.

Co-immunoprecipitation assay

Briefly, 2×10^6 CD19-WT or CD19-1XX CAR-expressing Jurkat cells were mixed with 1×10^6 $3T3^{CD19+}$ cells at room temperature. After the co-culture, the cells were resuspended in lysis buffer[38] on ice for 30 min, and centrifuged at 14000 g for 30 min to remove insoluble materials. The soluble cell lysate was mixed with anti-HA-beads and incubated for 3 h at 4℃ to immunoprecipitate HA-tagged CARs. After rinsed with wash buffer,[38] the immunoprecipitated proteins were eluted with SDS sample buffer, subjected to SDS-PAGE, and immunoblotted with the indicated antibodies.

Western Blot assay

The protein lysate was normalized according to the amount of CAR expression and resolved on 4% - 15% SDS polyacrylamide gel electrophoresis gels (SDS-PAGE, Bio-Rad). After protein transfer onto Polyvinylidene fluoride membranes (Bio-Rad), membranes were blocked in 5% bovine albumin in TBS-T and incubated with primary and secondary Abs in TBS-T with 2% bovine albumin. The following Abs were used: α-SHP1, α-HA tag and α-GAPDH (all from Cell Signaling Technology), horseradish peroxidase conjugated secondary Abs (Goat-anti-Rabbit from Thermo Scientific). Then the membrane was incubated with the primary antibody at 4°C overnight,

followed by incubation with the secondary antibody at room temperature for 1 hour. Lastly, the membrane was visualized with standard chemiluminescence.

Live cell imaging with FRET-based biosensors

The CD19 CAR-T cells expressing biosensors were generated by the lentivirus transduction of the Jurkat T cells.[17] For imaging of CAR signaling upon antigen stimulation, CAR-T cells were dropped on the glass-bottom dishes that have been coated with the NIH-3T3 cells expressing CD19 antigens. The time-lapse fluorescence images were taken with a Nikon Eclipse Ti inverted microscope at an interval of 30 s. The W-VIEW GEMINI imaging splitting optics (Hamamatsu, Japan) with an iXon Ultra 897 camera was used to capture the ECFP (a 474/40 nm emission filter) and FRET (a 535/25 nm emission filter) fluorescent signals simultaneously. During imaging, the cells were maintained with 5% CO_2 at 37 °C using the Tokai Hit ST Series Stage Top Incubator (Tokai Hit, Japan).

Mouse systemic tumor model

Six to eight week old NOD/SCID/IL-2Rγ null (NSG) mice (Shanghai Jihui, China) were used. All mice were housed at the Westlake University under pathogen-free conditions, and all procedures were approved by the ethical committee of Westlake University. Mice were subcutaneously (s.c.) injected a total of 1×10^6 target tumor cells (Panc-1^{CD19+} or A375) into the right flanks. Seven days later 1×10^6 CD19-specific or 2.5×10^6 AXL-specific CAR-T cells were injected. Tumor size was recorded every 3-4 days using a vernier caliper. Tumor volume was calculated as follows: tumor volume = long diameter × (short diameter^2)/2. NSG mice were euthanized when the tumor size exceeded 14mm (Panc-1^{CD19+} model) or 19mm (A375 model), so Panc-1^{CD19+} model mice were euthanized and the tissue was harvested 53 days after CAR-T cell injection. A375 model mice were euthanized and the tissue was harvested 26 days after CAR-T cell injection. For each group,

3-5 individual mice were included. Stratified randomization based on the initial tumor size was used. No animal data were excluded in this study. No strategy was used to minimize potential confounders. D.Y and J.C. were aware of the group allocation at the different stages of the experiment.

Statistical analysis

Unpaired Student *t* tests or one-way ANOVA (with the appropriate multiple comparisons test) was carried out using the GraphPad Prism version 7.0 (GraphPad Software Inc). ns, $P > 0.05$; *, $P < 0.05$; **, $P < 0.01$; ***, $P < 0.001$ and ****, $P < 0.0001$.

Abbreviations

ITAMs: Immunoreceptor tyrosine-based activation motifs; CAR-T: Chimeric antigen receptor engineered T cells; WT: Wild type; CFSE: Carboxyfluorescein diacetate succinimidyl ester; IFN: Interferon; IL: Interleukin; TNF: Tumor necrosis factor; FRET: Fluorescence resonance energy transfer; Co-IP: Co-Immunoprecipitation; WB: Western Blot; IB: Immunoblot; Lck: leukocyte-specific protein tyrosine kinase; SHP1: Src-Homology 2 domain Phosphatase-1; ZAP70: 70-kDa zeta-associated protein; Ca^{2+}: Calcium; Erk: Extracellular-regulated protein kinases; FBS: Fetal bovine serum; DMEM: Dulbecco's Modified Eagle Medium; RPMI: Roswell Park Memorial Institute, DAG: Diacylglycerol; IP3: Inositol 1,4,5-trisphosphate; PIP3: Phosphatidylinositol 3,4,5-trisphosphate.

Acknowledgment

This research was funded by the National Key R&D Program of China 2021YFA0909900 (J.S.), the National Natural Science Foundation of China grants 31971324 (J.S.), 82161138028 (J.S.), 81973993 (X.G.), Zhejiang Provincial Natural Science Foundation grant LR20H160003 (J.S.), LR20C070001 (X.G.) and the Leading Innovative and Entrepreneur Team Introduction Program

of Zhejiang grant 2020R01006 (J.S.). The authors thank the support of Zhejiang Provincial Key Laboratory of Immunity and Inflammatory diseases and Zhejiang University School of Medicine core facilities. We also thank Courtney R. Kwong for editing the manuscript.

Authors' contributions

Y.D. and J.S. designed the studies and conceived the experiments. Y.D., J.C. and X.M. performed most of the experiments; L.L., K.S., X.W., Y.W., Z.H. and H.L. conducted data analysis; Y.D. and J.S. wrote the manuscript. Y.H., C.Z., X.G. and Y.W. discussed the manuscript, X.G., J.S. were responsible for funding acquisition. All authors read and approved the final manuscript.

Declaration of interests

A patent application related to this study on which J.S. is named as an inventor has been approved. The other authors declare no competing interests.

References

1. Duan Y, Chen R, Huang Y, Meng X, Chen J, Liao C, Tang Y, Zhou C, Gao X, Sun J. (2021). Tuning the ignition of CAR: optimizing the affinity of scFv to improve CAR-T therapy. Cell Mol Life Sci. 79, 14. https://doi.org/10.1007/s00018-021-04089-x.
2. Manier S, Ingegnere T, Escure G, Prodhomme C, Nudel M, Mitra S, Facon T. (2022). Current state and next-generation CAR-T cells in multiple myeloma. Blood Rev. 54, 100929. https://doi.org/10.1016/j.blre.2022.100929.
3. Hou AJ, Chen LC, Chen YY. (2021). Navigating CAR-T cells through the solid-tumour microenvironment. Nat Rev Drug Discov. 20, 531-550. https://doi.org/10.1038/s41573-021-00189-2.
4. Guo Y, Xie YQ, Gao M, Zhao Y, Franco F, Wenes M, Siddiqui I, Bevilacqua A, Wang H, Yang H, et al. (2021). Metabolic reprogramming of terminally exhausted CD8+ T cells by IL-10 enhances anti-tumor immunity. Nat Immunol. 22, 746-756. https://doi.org/10.1038/s41590-021-00940-2.
5. Agliardi G, Liuzzi AR, Hotblack A, De Feo D, Núñez N, Stowe CL, Friebel E, Nannini F, Rindlisbacher L, Roberts TA, et al. (2021). Intratumoral IL-12 delivery empowers CAR-T cell immunotherapy in a pre-clinical model of glioblastoma. Nat Commun. 12, 444. https://doi.org/10.1038/s41467-020-20599-x.
6. Rafiq S, Yeku OO, Jackson HJ, Purdon TJ, van Leeuwen DG, Drakes DJ, Song M, Miele MM, Li Z, Wang P, et al. (2018). Targeted delivery of a PD-1-blocking scFv by CAR-T cells enhances anti-tumor efficacy in vivo. Nat Biotechnol. 36, 847-856. https://doi.org/10.1038/nbt.4195.
7. Choi BD, Yu X, Castano AP, Bouffard AA, Schmidts A, Larson RC, Bailey SR, Boroughs AC, Frigault MJ, Leick MB, et al. (2019). CAR-T cells secreting BiTEs circumvent antigen escape without detectable toxicity. Nat Biotechnol. 37, 1049-1058. https://doi.org/10.1038/s41587-019-0192-1.

8. Adachi K, Kano Y, Nagai T, Okuyama N, Sakoda Y, Tamada K. (2018). IL-7 and CCL19 expression in CAR-T cells improves immune cell infiltration and CAR-T cell survival in the tumor. Nat Biotechnol. 36, 346-351. https://doi.org/10.1038/nbt.4086.
9. Kershaw MH, Westwood JA, Darcy PK. (2013). Gene-engineered T cells for cancer therapy. Nat Rev Cancer. 13, 525-41. https://doi.org/10.1038/nrc3565.
10. Lo WL, Shah NH, Ahsan N, Horkova V, Stepanek O, Salomon AR, Kuriyan J, Weiss A. (2018). Lck promotes Zap70-dependent LAT phosphorylation by bridging Zap70 to LAT. Nat Immunol. 19, 733-741. https://doi.org/10.1038/s41590-018-0131-1.
11. Navarro MN, Cantrell DA. (2014). Serine-threonine kinases in TCR signaling. Nat Immunol. 15, 808-14. https://doi.org/10.1038/ni.2941.
12. Michel F, Attal-Bonnefoy G, Mangino G, Mise-Omata S, Acuto O. (2001). CD28 as a molecular amplifier extending TCR ligation and signaling capabilities. Immunity. 15, 935-45. https://doi.org/10.1016/s1074-7613(01)00244-8.
13. Esensten JH, Helou YA, Chopra G, Weiss A, Bluestone JA. (2016). CD28 Costimulation: From Mechanism to Therapy. Immunity. 44, 973-88. https://doi.org/10.1016/j.immuni.2016.04.020.
14. Min L, Joseph RE, Fulton DB, Andreotti AH. (2009). Itk tyrosine kinase substrate docking is mediated by a nonclassical SH2 domain surface of PLCgamma1. Proc Natl Acad Sci U S A. 106, 21143-8. https://doi.org/10.1073/pnas.0911309106.
15. Takesono A, Finkelstein LD, Schwartzberg PL. (2002). Beyond calcium: new signaling pathways for Tec family kinases. J Cell Sci. 115, 3039-48. https://doi.org/10.1242/jcs.115.15.3039.
16. Feucht J, Sun J, Eyquem J, Ho YJ, Zhao Z, Leibold J, Dobrin A, Cabriolu A, Hamieh M, Sadelain M. (2019). Calibration of CAR activation potential directs alternative T cell fates and therapeutic potency. Nat Med. 25, 82-88. https://doi.org/10.1038/s41591-018-0290-5.
17. Liu L, Limsakul P, Meng X, Huang Y, Harrison RES, Huang TS, Shi Y, Yu Y, Charupanit K, Zhong S, et al. (2021). Integration of FRET and sequencing to engineer kinase biosensors from mammalian cell libraries. Nat Commun. 12, 5031. https://doi.org/10.1038/s41467-021-25323-x.
18. Kim TJ, Seong J, Ouyang M, Sun J, Lu S, Hong JP, Wang N, Wang Y. (2009). Substrate rigidity regulates Ca^{2+} oscillation via RhoA pathway in stem cells. J Cell Physiol. 218, 285-93. https://doi.org/10.1002/jcp.21598.
19. Komatsu N, Aoki K, Yamada M, Yukinaga H, Fujita Y, Kamioka Y, Matsuda M. (2011). Development of an optimized backbone of FRET biosensors for kinases and GTPases. Mol Biol Cell. 22, 4647-56. https://doi.org/10.1091/mbc.e11-01-0072.
20. Eyquem J, Mansilla-Soto J, Giavridis T, van der Stegen SJ, Hamieh M, Cunanan KM, Odak A, Gönen M, Sadelain M. (2017). Targeting a CAR to the TRAC locus with CRISPR/Cas9 enhances tumour rejection. Nature. 543, 113-117. https://doi.org/10.1038/nature21405.
21. Zhao Z, Condomines M, van der Stegen SJC, Perna F, Kloss CC, Gunset G, Plotkin J, Sadelain M. (2015). Structural Design of Engineered Costimulation Determines Tumor Rejection Kinetics and Persistence of CAR T Cells. Cancer Cell. 28, 415-428. https://doi.org/10.1016/j.ccell.2015.09.004.
22. Boshuizen J, Koopman LA, Krijgsman O, Shahrabi A, van den Heuvel EG, Ligtenberg MA, Vredevoogd DW, Kemper K, Kuilman T, Song JY, et al. (2018). Cooperative targeting of melanoma heterogeneity with an AXL antibody-drug conjugate and BRAF/MEK inhibitors. Nat Med. 24, 203-212. https://doi.org/10.1038/nm.4472.
23. Wan R, Wu J, Ouyang M, Lei L, Wei J, Peng Q, Harrison R, Wu Y, Cheng B, Li K, et al. (2019). Biophysical basis underlying dynamic Lck activation visualized by ZapLck FRET biosensor. Sci Adv. 5, eaau2001. https://doi.org/10.1126/sciadv.aau2001.
24. Jiangyue Liu, Xianhui Chen, Jason Karlen, Alfonso Brito, Tiffany Jheng, Philippe Foubert, Janani Krishnamurthy, Yannick Bulliard, Blake Aftab. (2020). 98 ATA3271: An armored, next-generation off-the-shelf, allogeneic, mesothelin-CAR T cell therapy for solid tumors. Journal for ImmunoTherapy of Cancer, 8. http://dx.doi.org/10.1136/jitc-2020-SITC2020.0098.
25. Rohrs JA, Siegler EL, Wang P, Finley SD. (2020). ERK Activation in CAR T Cells Is Amplified by CD28-Mediated Increase in CD3ζ Phosphorylation. iScience. 23, 101023. https://doi.org/10.1016/j.isci.2020.101023.
26. Raab M, Cai YC, Bunnell SC, Heyeck SD, Berg LJ, Rudd CE. (1995). p56Lck and p59Fyn regulate CD28 binding to phosphatidylinositol 3-kinase, growth factor receptor-bound protein GRB-2, and T cell-specific

protein-tyrosine kinase ITK: implications for T-cell costimulation. Proc Natl Acad Sci U S A. 92, 8891-5. https://doi.org/10.1073/pnas.92.19.8891.
27. Sadra A, Cinek T, Arellano JL, Shi J, Truitt KE, Imboden JB. (1999). Identification of tyrosine phosphorylation sites in the CD28 cytoplasmic domain and their role in the costimulation of Jurkat T cells. J Immunol. 162, 1966-73. https://pubmed.ncbi.nlm.nih.gov/9973466/.
28. Trebak M, Kinet JP. (2019). Calcium signalling in T cells. Nat Rev Immunol. 19, 154-169. https://doi.org/10.1038/s41577-018-0110-7.
29. Meng X, Wu X, Zheng Y, Shang K, Jing R, Jiao P, Zhou C, Zhou J, Sun J. (2020). Exploiting Ca2+ signaling in T cells to advance cancer immunotherapy. Semin Immunol. 49, 101434. https://doi.org/10.1016/j.smim.2020.101434.
30. Foletta VC, Segal DH, Cohen DR. (1998). Transcriptional regulation in the immune system: all roads lead to AP-1. J Leukoc Biol. 63, 139-52. https://doi.org/10.1002/jlb.63.2.139.
31. Lavoie H, Gagnon J, Therrien M. (2020). ERK signalling: a master regulator of cell behaviour, life and fate. Nat Rev Mol Cell Biol. 21, 607-632. https://doi.org/10.1038/s41580-020-0255-7.
32. Xie X, Zhu L, Jie Z, Li Y, Gu M, Zhou X, Wang H, Chang JH, Ko CJ, Cheng X, Sun SC. (2021). TRAF2 regulates T cell immunity by maintaining a Tpl2-ERK survival signaling axis in effector and memory CD8 T cells. Cell Mol Immunol. 18, 2262-2274. https://doi.org/10.1038/s41423-020-00583-7.
33. Mele F, Basso C, Leoni C, Aschenbrenner D, Becattini S, Latorre D, Lanzavecchia A, Sallusto F, Monticelli S. (2015). ERK phosphorylation and miR-181a expression modulate activation of human memory TH17 cells. Nat Commun. 6, 6431. https://doi.org/10.1038/ncomms7431.
34. Damasio MP, Marchingo JM, Spinelli L, Hukelmann JL, Cantrell DA, Howden AJM. (2021). Extracellular signal-regulated kinase (ERK) pathway control of CD8+ T cell differentiation. Biochem J. 478, 79-98. https://doi.org/10.1042/bcj20200661.
35. Brentjens RJ, Latouche JB, Santos E, Marti F, Gong MC, Lyddane C, King PD, Larson S, Weiss M, Rivière I, et al. (2003). Eradication of systemic B-cell tumors by genetically targeted human T lymphocytes co-stimulated by CD80 and interleukin-15. Nat Med. 9, 279-86. https://doi.org/10.1038/nm827.
36. Jing R, Jiao P, Chen J, Meng X, Wu X, Duan Y, Shang K, Qian L, Huang Y, Liu J, et al. (2021). Cas9-Cleavage Sequences in Size-Reduced Plasmids Enhance Nonviral Genome Targeting of CARs in Primary Human T Cells. Small Methods. 5, e2100071. https://doi.org/10.1002/smtd.202100071.
37. Duan Y, Luo L, Qiao C, Li X, Wang J, Liu H, Zhou T, Shen B, Lv M, Feng J. (2019). A novel human anti-AXL monoclonal antibody attenuates tumour cell migration. Scand J Immunol. 90, e12777. https://doi.org/10.1111/sji.12777.
38. Wu W, Zhou Q, Masubuchi T, Shi X, Li H, Xu X, Huang M, Meng L, He X, Zhu H, et al. (2020). Multiple Signaling Roles of CD3ε and Its Application in CAR-T Cell Therapy. Cell. 182, 855-871. https://doi.org/10.1016/j.cell.2020.07.018.

Figure legends

Figure 1. CD19-1XX CAR-T cells show reduced cytotoxicity but enhanced proliferation *in vitro*.

(a) Targeting of CD19-WT or CD19-1XX CAR into the *TRAC* locus by CRISPR/Cas9. (b)FACS analysis showing the expression levels of two CD19 CARs. Data are representative of at least three independent experiments with similar results. Untransduced T cells were used as the control. (c) Normalized CD19-WT and CD19-1XX CAR expression (n=3, for each donor, MFI value of 1XX CAR was normalized to MFI of WT CAR). (d) Cytotoxic activity of CD19-WT and CD19-1XX CAR-T cells using an 18 h bioluminescence assay with FFL-expressing Panc-1^{CD19+} cells as targets. (n=3, 1 experiment performed in triplicates from 1 donor). (e) Normalized lysis of target cells by CD19-WT or CD19-1XX CAR-T cells at E:T=1:1 (n=9, 3 independent experiments performed in triplicates from 3 donors). (f) Normalized cytokine secretion of CD19-WT and CD19-1XX cells were detected after stimulation by target cells. (E:T=4:1, n=9, 3 independent experiments performed in triplicates from 3 donors). For each donor, cytokine secretion by 1XX CAR was normalized to that secreted by WT CAR. (g) The proliferation of CD19-WT and CD19-1XX CAR-T cells analyzed by CSFE assay. Unstim represents CAR-T cells without 3T3^{CD19+} cell coculture and stim represents CAR-T cells stimulated with 3T3^{CD19+} cells for 72h. (E:T=4:1, n=3, 1 experiment performed in triplicates from 1 donor). (h) CAR-T cell antigen-dependent proliferation fold calculated by stim/unstim ratio (E:T=4:1, n=9, 3 experiment performed in triplicates from 3 donors). All data are mean ± SD.

Figure 2. CD19-1XX CAR-T cells show better anti-tumor activity in a pancreatic tumor model *in vivo*.

(a) Timeline of CD19 CAR-T treatment in the mouse model. (b) Panc-1^{CD19+} -bearing mice were treated with 1×10^6 CD19 CAR-T cells as indicated, and the tumor burden (tumor volume) of mice

was measured at indicated days (n=4 mice each group). For mouse experiments, Control used PBS. (c) Tumor tissue from mice treated with indicated CAR-T cells. (d) Tumor tissue from mice treated with indicated CAR-T cells was sliced and stained with antibodies against human CD4 and CD8 (n=4). The percentage of $CD4^+$ (e) and $CD8^+$ (f) T cells in tumor tissue from different groups of mice (n=4). Number of $CD4^+$ CAR-T cells (g), $CD8^+$ CAR-T cells (h) in the spleen of mice 53 days post CAR-T infusion (n=5). (i, j) Phenotype of CAR-T cells in the spleen of mice 53 days after CAR-T infusion as demonstrated by the percentage of T_{CM} ($CD45RA^-CD62L^+$) and T_{EFF} ($CD45RA^+CD62L^-$) cells (n=5). All data are mean ± SD.

Figure 3. 1XX modification of AXL CAR reduced cytotoxicity but enhanced proliferation *in vitro*. (a) Targeting of AXL-WT or AXL-1XX into the *TRAC* locus by CRISPR/Cas9. (b) FACS analysis showing the expression levels of two AXL CARs. Data are representative of at least three independent experiments with similar results. Untransduced T cells were used as the control. (c) Normalized CD19 WT and 1XX CAR expression (n=3, for each donor, MFI value of 1XX CAR was normalized to MFI of WT CAR). (d) Cytotoxic activity of AXL-WT and AXL- 1XX using an 18 h bioluminescence assay with FFL-expressing A375 cells as targets. (n=3, 1 experiment performed in triplicates from 1 donor). (e) Normalized lysis of target cells by AXL-WT or AXL-1XX CAR-T cells at E:T=1:1 (n=9, 3 independent experiments performed in triplicates from 3 donors). (f) Normalized cytokine secretion of AXL-WT and AXL-1XX were detected 24h after stimulation by target cells (E:T=4:1, n=9, 3 independent experiments performed in triplicates from 3 donors). For each donor, cytokine secretion by 1XX CAR was normalized to that secreted by WT CAR. (g) The proliferation of AXL-WT and AXL-1XX CAR-T cells analyzed by CSFE assay. Unstim represents CAR-T cells without target cell coculture and Stim represents CAR-T cells stimulated with target cells for 72h. (E:T=4:1, n=3, 1 experiment performed in triplicates from 1

donor). (h) CAR-T cell antigen-dependent proliferation fold calculated by Stim/Unstim ratio (E:T=4:1, n=9, 3 experiment performed in triplicates from 3 donors). All data are mean ± SD.

Figure 4. 1XX modification of the AXL CAR enhance its anti-tumor activity in a melanoma tumor model.

(a) Timeline of of the AXL CAR-T treatment in the mouse model. (b) A375-bearing mice were treated with 2.5×10^6 AXL CAR-T cells and the tumor burden (tumor volume) of mice were measured at the indicated days (n=4, 5, 5 mice in respective groups). Control, PBS. (c) Tumor tissue of the mice treated with indicated CAR-T cells (n=4, 5, 5). (d) The weight of the tumors from different groups of mice (n=4, 5, 5). (e) Tumor tissue from the mice treated with indicated CAR-T cells was sliced and stained with antibodies against human CD4 and CD8 (n=5). The percentage of $CD4^+$ (f) and $CD8^+$ (g) T cells in tumor tissue from the different groups of mice (n=5). The number of $CD4^+$ CAR-T cells (h) and $CD8^+$ CAR-T cells (i) in the spleen of mice 26 days post CAR-T infusion (n=5, 3). (j, k). The phenotype of CAR-T cells in the spleen of mice 26 days after CAR-T infusion as demonstrated by the percentage of T_{CM} ($CD45RA^-CD62L^+$) and T_{EFF} ($CD45RA^+CD62L^-$) cells (n=5, 3). All data are mean ± SD.

Figure 5. CAR-mediated signaling dynamics in 1XX and WT CAR-T cells revealed by FRET biosensors.

(a) Schematic drawings of the constructs. The ZAP70-FRET biosensor was co-expressed with WT or 1XX CAR in Jurkat T cells. The CAR-T cells were then dropped onto the $3T3^{CD19+}$ cells to monitor the dynamic ZAP70 kinase activations. (b) Representative images of the ZAP70 biosensor in the T cells after attaching to the $3T3^{CD19+}$ cell monolayer. Scale bar,10 μm. (c) Time courses of

the ECPF/FRET ratio of the ZAP70 FRET biosensor in WT or 1XX CAR-T cells (n=13, 13). (d) Time courses of normalized ECFP/FRET ratio of the ZAP70 FRET biosensor in WT or 1XX CAR-T cells from 0-5 min (n=13, 13). (e) Normalized ECPF/FRET ratio of the ZAP70-FRET biosensor in WT or 1XX CAR-T cells at 2 min (n=13, 13, unpaired two-tailed Student's t-test, ns, $P > 0.05$). (f) Schematic drawings of constructs. The Ca^{2+}-FRET biosensor was co-expressed with WT or 1XX CAR in Jurkat T cells. The CAR-T cells were then dropped onto the $3T3^{CD19+}$ cells to monitor the dynamic Ca^{2+} kinase activations. (g) Representative images of the Ca^{2+} biosensor in T cells after attaching to the $3T3^{CD19+}$ cell monolayer. Scale bar,10 μm. (h) Time courses of FRET/ECFP ratio of Ca^{2+}-FRET biosensor in WT or 1XX CAR-T cells (n=27, 22). (i) Time courses of FRET/ECPF ratio of Ca^{2+}-FRET biosensor in WT or 1XX CAR-T cells from 0-3 min (n=27, 22). (j) FRET/ECFP ratio of Ca^{2+}-FRET biosensor in WT or 1XX CAR-T cells at 1.5 min (n=27, 22, unpaired two-tailed Student's t-test, **, $P < 0.01$). (k) Schematic drawings of constructs. The Erk-FRET biosensor was co-expressed with WT or 1XX CAR in Jurkat T cells. The CAR-T cells were then dropped onto the $3T3^{CD19+}$ cells to monitor the dynamic Erk kinase activations. (l) Representative images of the Erk biosensor in T cells after attaching to the $3T3^{CD19+}$ cell monolayer. Scale bar,10 μm. (m) Time courses of the normalized FRET/ECPF ratio of the Erk-FRET biosensor in WT or 1XX CAR-T cells (n=29, 29). (n) Time courses of the normalized FRET/ECPF ratio of the Erk-FRET biosensor in WT or 1XX CAR-T cells from 0-5 min (n=29, 29). (o) Normalized FRET/ECPF ratio of the Erk-FRET biosensor in WT or 1XX CAR-T cells at 1.5 min (n=29, 29, **, $P < 0.01$). All data are mean ± SEM.

Figure 6. Signaling dynamics of the three key molecules downstream WT (left) and 1XX (right) CAR activation. Upon CAR binding to antigen, Lck phosphorylates CD28 and CD3ζ signaling

domains. Doubly-phosphorylated ITAMs recruit ZAP70 and ZAP70 gets activated by Lck. Singly-phosphorylated ITAMs recruit Shp1 to inhibit Lck by negative feedback. Activated ZAP70 phosphorylates LAT subsequently activates both Ca^{2+} and Erk. Phosphorylated CD28 also activates Ca^{2+} and Erk through the PI3K pathway. In 1XX, reduced ITAMs lead to decreased Shp1 inhibition and possibly enhanced Lck activity. Thus, the PI3K-dependent Ca^{2+} and Erk pathway gets strengthened. Net ZAP70 activity remains unaltered from two opposing effects: decreased ZAP70 binding from reduced ITAMs, and increased ZAP70 phosphorylation by Lck.

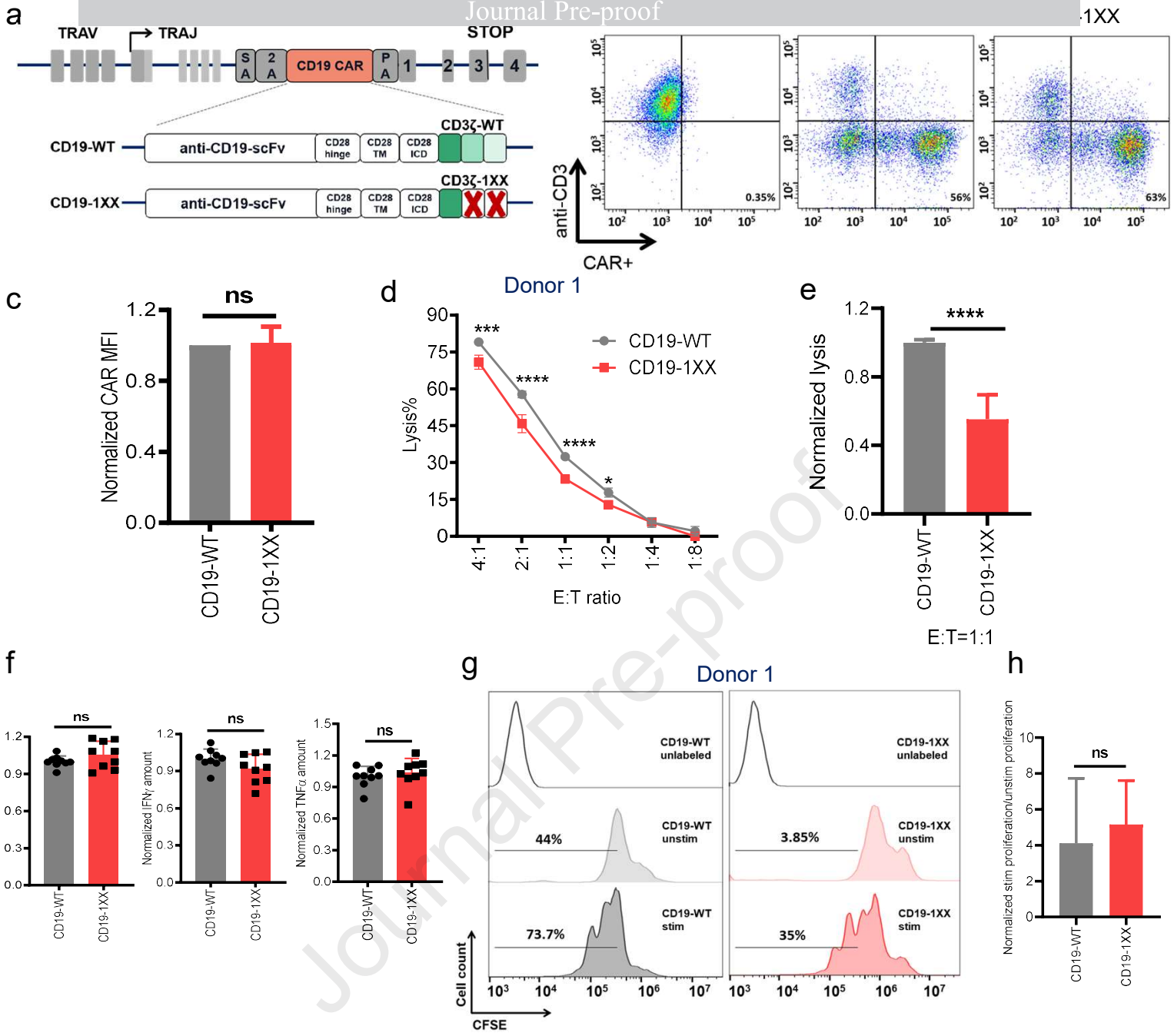

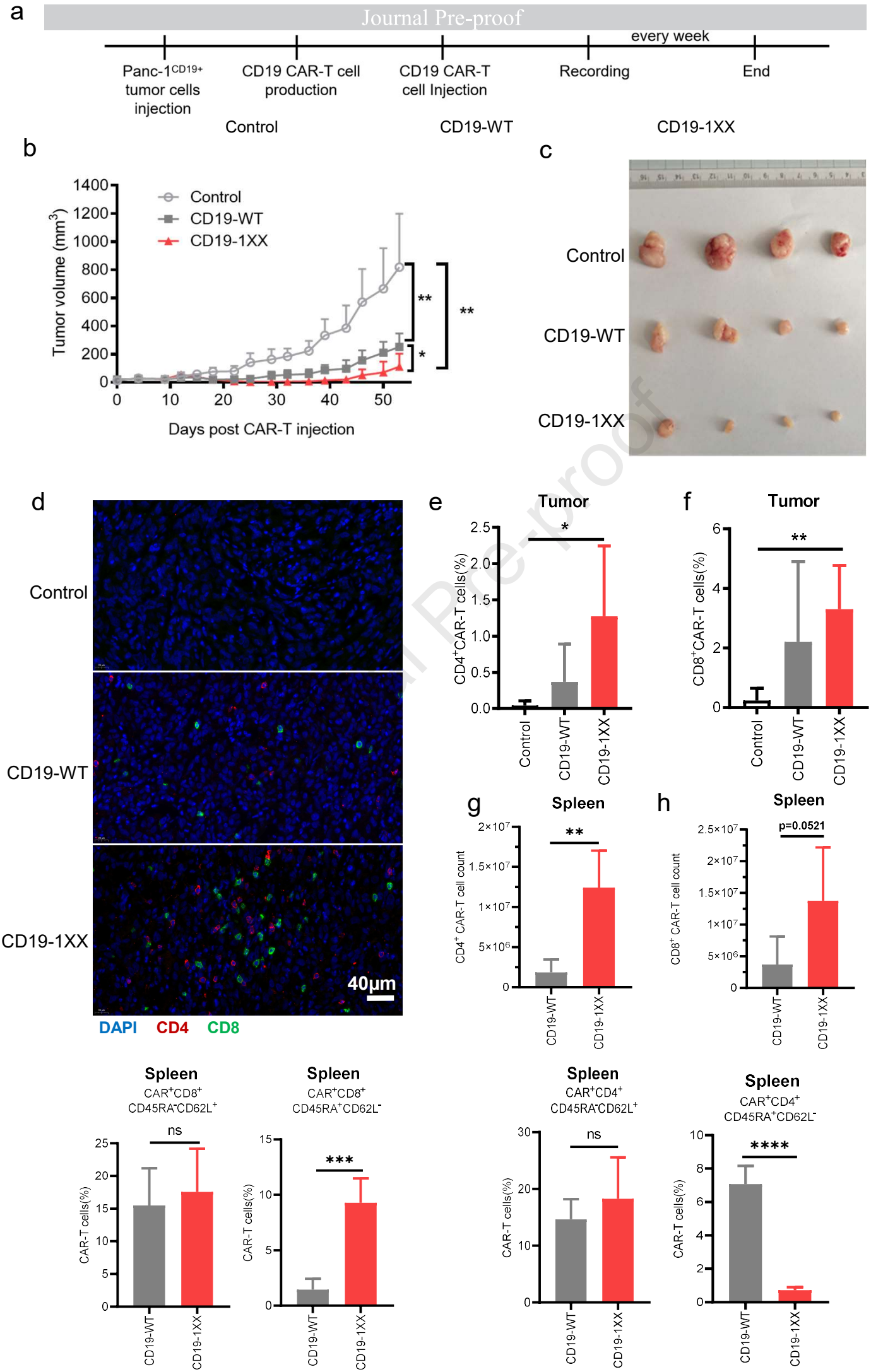

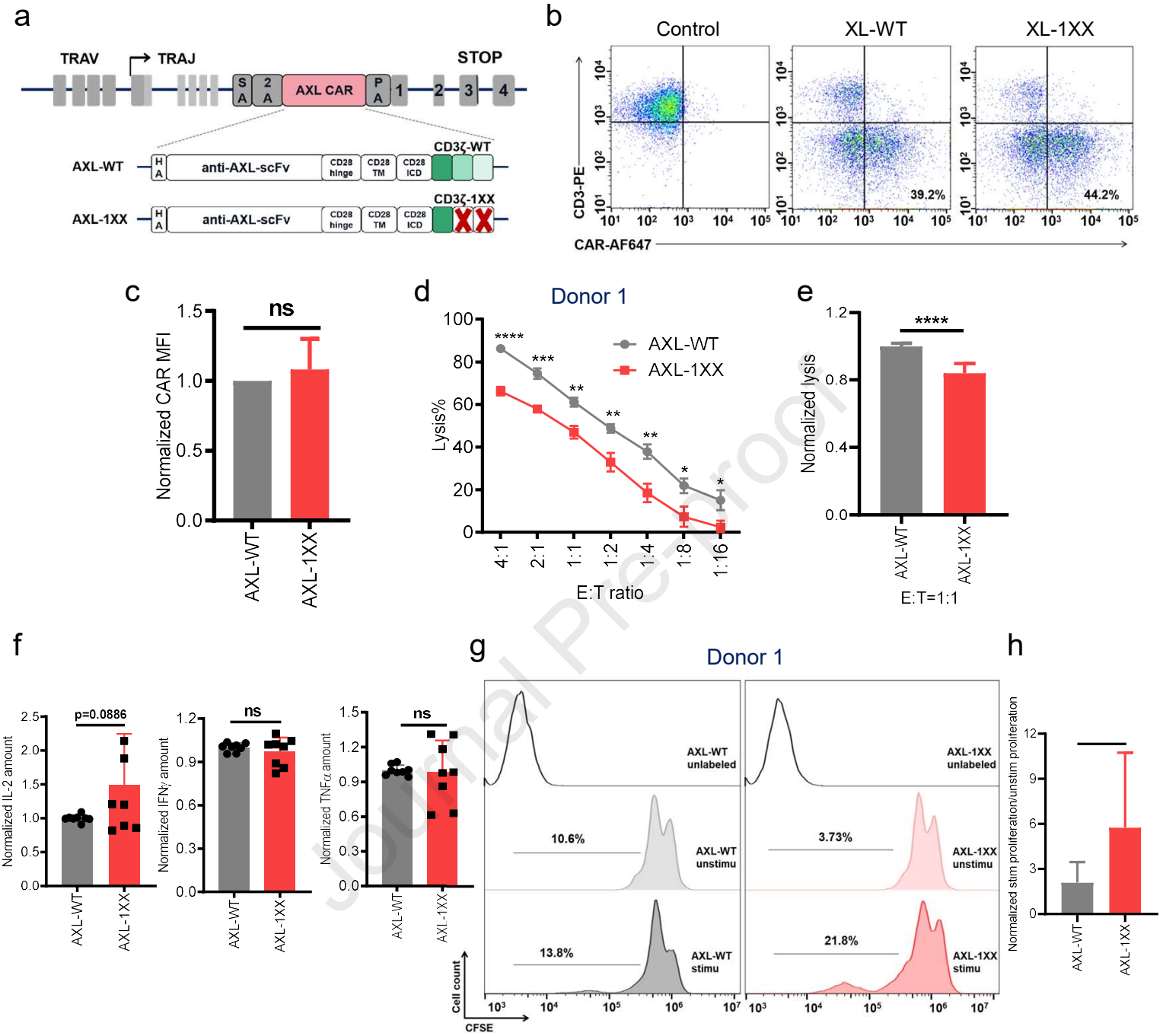
a
TRAV
TRAJ
STOP
S A
2 A
AXL CAR
P A
1
2
3
4
AXL-WT
H A
anti-AXL-scFv
CD28 hinge
CD28 TM
CD28 ICD
CD3ζ-WT
AXL-1XX
CD3ζ-1XX
b
Control
XL-WT
XL-1XX
CD3-PE
CAR-AF647
39.2%
44.2%
c
ns
Normalized CAR MFI
AXL-WT
AXL-1XX
d
Donor 1
AXL-WT
AXL-1XX
Lysis%
E:T ratio
4:1
2:1
1:1
1:2
1:4
1:8
1:16
e
****
Normalized lysis
E:T=1:1
f
p=0.0886
ns
ns
Normalized IL-2 amount
Normalized IFNγ amount
Normalized TNFα amount
g
Donor 1
AXL-WT unlabeled
AXL-1XX unlabeled
10.6%
AXL-WT unstimu
3.73%
AXL-1XX unstimu
13.8%
AXL-WT stimu
21.8%
AXL-1XX stimu
Cell count
CFSE
h
Normalized stim proliferation/unstim proliferation

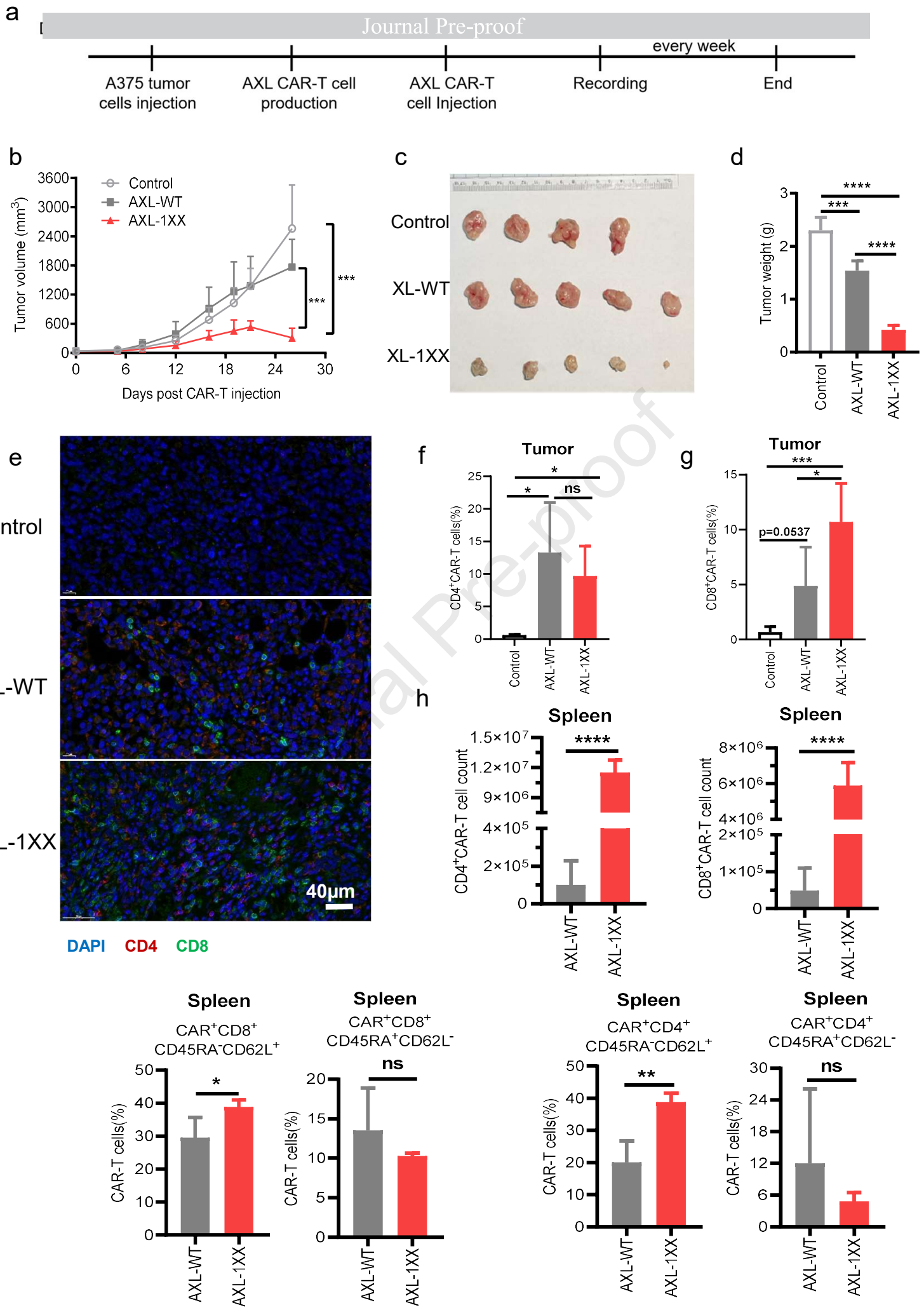

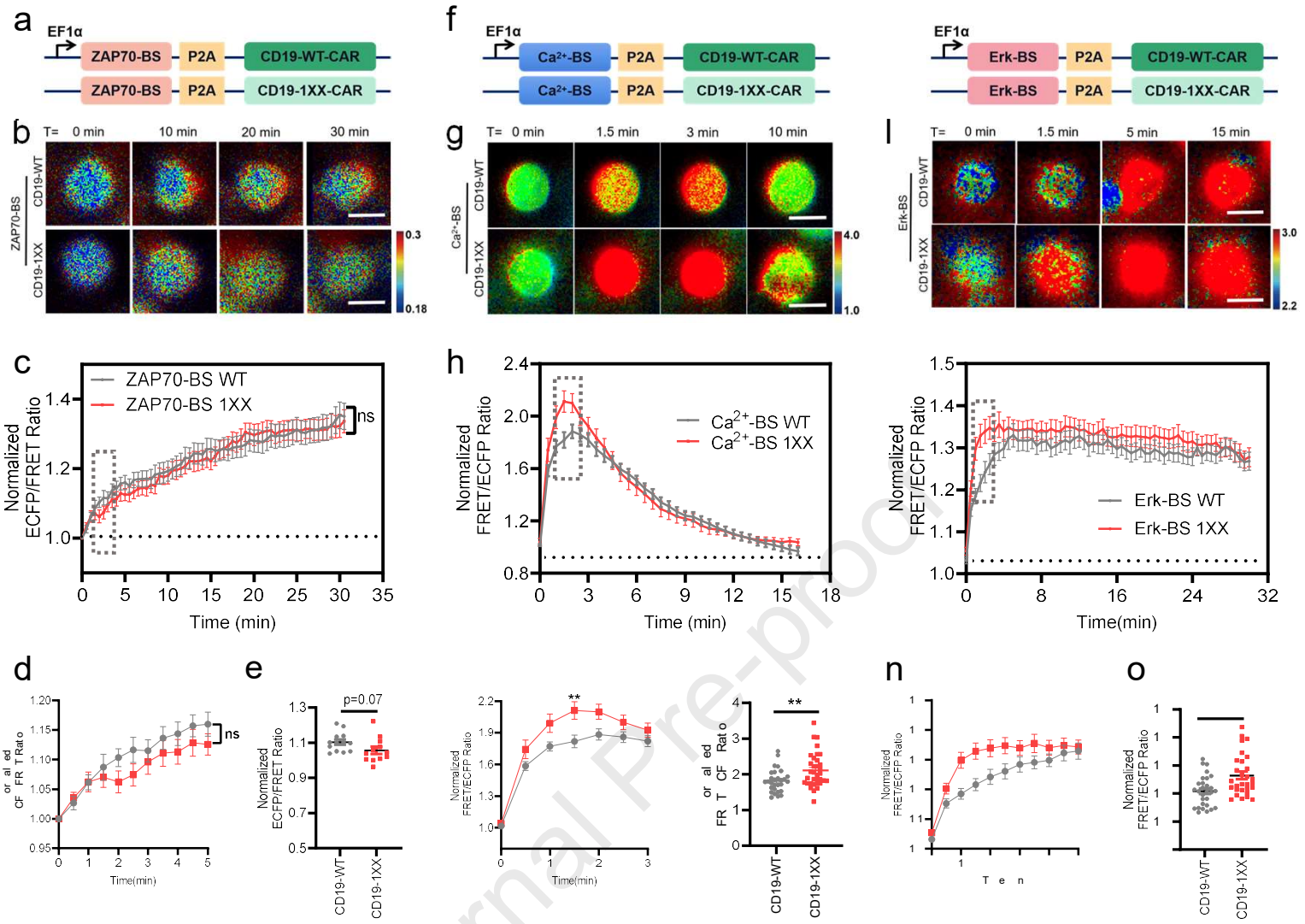

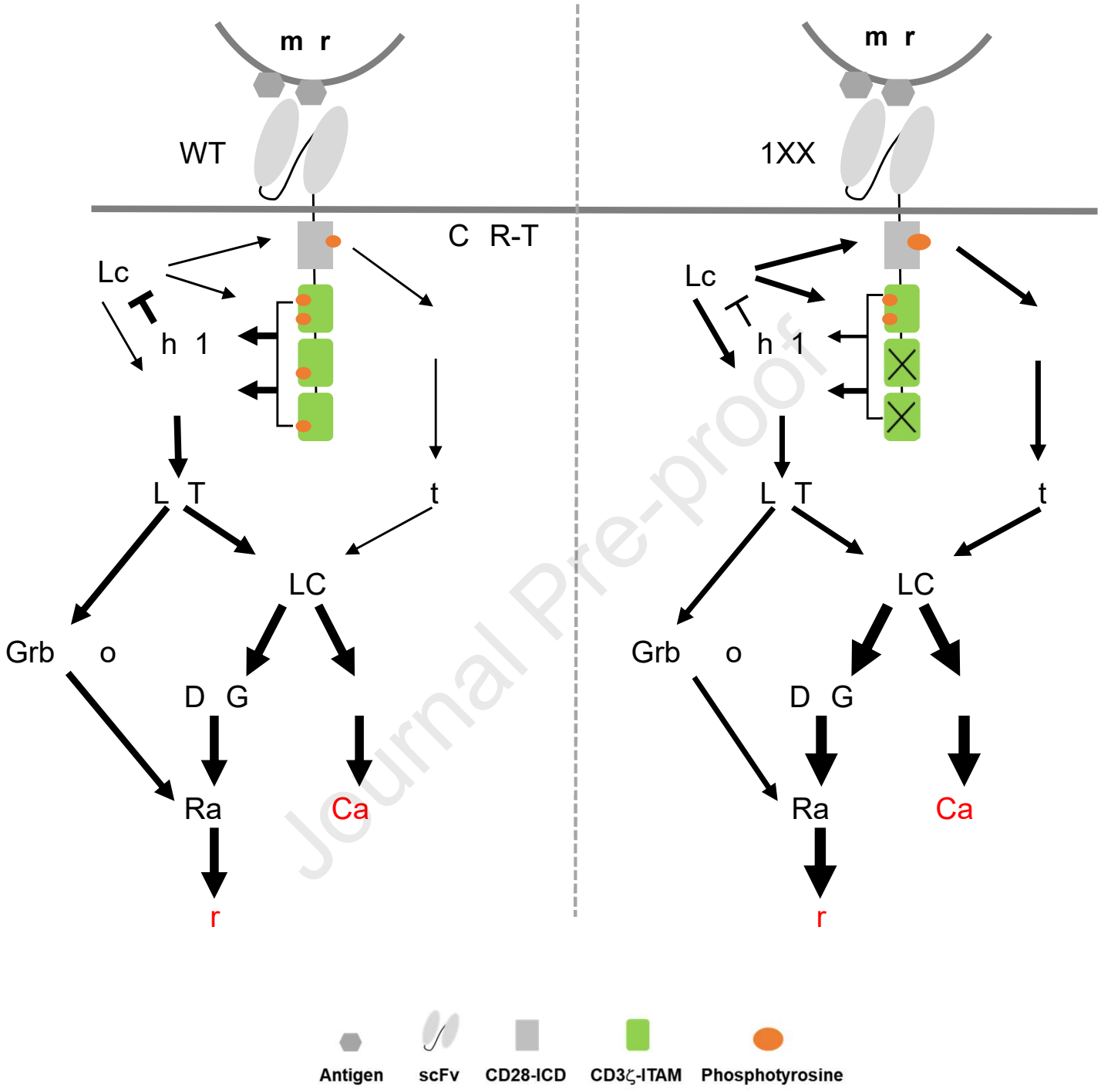

A single-ITAM containing 1XX CAR displayed superior anti-tumor activity in two solid tumor models than WT CAR, paving the way for its clinical applications against solid tumors. Imaging with FRET-based biosensors revealed that 1XX induced higher Ca^{2+} elevation and faster Erk activation possibly through reduced Shp1 association and enhanced Lck activation.